Engineering Fracture Mechanics 77 (2010) 3359–3367

Contents lists available at ScienceDirect

Engineering Fracture Mechanics

journal homepage: www.elsevier.com/locate/engfracmech

Numerical investigations of the stepped double torsion fracture toughness specimen

M.S. Attia [a,*], A.S. Mahmoud [b], M.M. Megahed [a], A.A. Radwan [a]

[a] Department of Mechanical Design and Production, Faculty of Engineering, Cairo University, 12613-Giza, Egypt
[b] Department of Industrial Engineering, Faculty of Engineering, Fayoum University, 63514-Fayoum, Egypt

ARTICLE INFO

Article history:
Received 15 March 2010
Received in revised form 29 July 2010
Accepted 18 August 2010
Available online 25 August 2010

Keywords:
Fracture toughness
Double torsion
Stepped specimen
Finite element analysis

ABSTRACT

This study aims at investigating the fracture behaviour of double torsion specimens using the finite element method. Typical double torsion tests encompass a series of constant-thickness specimens to evaluate the material plane strain fracture toughness. In contrast, the concept of using a novel variable thickness stepped specimen aims at deducing the fracture toughness using a single specimen. In this work, the feasibility of this approach is examined and the effect of the number of steps and fracture thickness in a specimen upon the resulting conditional stress intensity factor is evaluated. The finite element models employed experimentally determined values of the fracture load to evaluate the conditional stress intensity factor of the specimen. Finite element predictions were compared with earlier experimental results using both cast aluminium silicon alloy and gray cast iron specimens and good matching was observed between experimental results and numerical predictions.

1. Introduction

The double torsion test (DT) has been introduced in the late sixties as a relatively simple and inexpensive technique to evaluate the fracture mechanics characteristics of both metallic and nonmetallic materials. Specifically, DT testing has been extensively used to study both plane strain fracture toughness "K_{IC}" evaluation and slow crack growth characteristics in situations where standard size requirements cannot be satisfied, such as thin sheets. The pioneering work of Outwater and Gerry [1,2] and Kies and Clark [3] laid the experimental foundation for this test methodology. The main characteristic of this technique is the independence of the stress intensity factor "K_I" from the crack length "a", thus making this test ideal for situations where it is difficult to measure the crack length during testing as in opaque materials or elevated temperature testing. Extensive research has since been devoted to investigate the various aspects of this technique [4–6].

Fig. 1 depicts a typical test configuration, in which a rectangular specimen with length "L", width "W", and thickness "t" rests on roller supports and is loaded by a force "P" in a four-point bending setup. This loading configuration enables a crack of length "a" along the symmetry plane of the two halves to incrementally propagate by increments "Δa". Hence, the developed two branches are loaded in torsion along the crack length by a torsional moment "M". Analytical treatment of this problem assumes that the width "W" is much larger than the thickness "t" and that the uncracked region is rigid, especially for moderately long cracks. These assumptions enable the well-known analytical solution of non-circular bars torsion to be applied to this problem [7–10]. Hence, the conditional stress intensity factor is given by:

* Corresponding author. Tel.: +1 416 323 9873; fax: +2 02 3567 8516.
E-mail address: m.attia@utoronto.ca (M.S. Attia).

0013-7944/$ - see front matter © 2010 Elsevier Ltd. All rights reserved.
doi:10.1016/j.engfracmech.2010.08.012

Nomenclature

E	Young's modulus
K_C	critical stress intensity factor for plane stress conditions
K_{IC}	plane strain fracture toughness
K_Q	conditional stress intensity factor
L	length of double torsion specimen
P_c	critical load
W	width of double torsion specimen
W_m	distance between supports of double torsion specimen
a	crack length
Δa	amount of increase of crack length
t	thickness of double torsion specimen
t_c	thickness between top and bottom grooves of double torsion specimen
v	Poisson's ratio

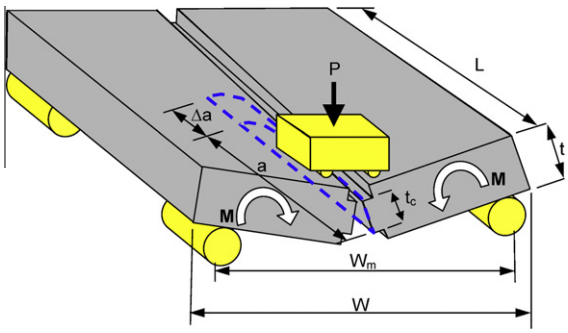

Fig. 1. Schematic of plain double torsion test specimen.

$$K_Q = \begin{cases} \frac{P_c W_m}{2}\sqrt{\frac{3(1+v)}{t^3 t_c W \psi}} & \text{for plane stress} \\ \frac{P_c W_m}{2}\sqrt{\frac{3}{t^3 t_c W \psi (1-v)}} & \text{for plane strain} \end{cases} \quad (1)$$

where ψ is a thickness correction function for thick beams [10] given by:

$$\psi = 1 - 0.6302\left(\frac{2t_c}{W}\right) + 1.2\left(\frac{2t_c}{W}\right)e^{-(\pi W/2t_c)} \quad (2)$$

Proper understanding of the mode of fracture and the applicable analytical model (plane stress/strain) is pivotal to standardizing the DT test. While it seems that the crack propagation is mode-III dominated, close agreement was found between experiments and analytical results using mode-I analysis [7,8]. Furthermore, previous studies employed both plane stress and plane strain models to evaluate the critical stress intensity factors [8,11] and compare to fracture toughness estimates using standard tests. A closer examination of Eq. (1) shows that the difference between the two models is dependent upon Poisson's ratio of the material. The validity of these assumptions will be assessed in the present work using three-dimensional finite element analyses.

Trantina [12] conducted the earliest three-dimensional FE simulations of the DT specimen using a bilinear crack front to approximate the actual curved front. This study aimed to investigate the effect of specimen geometry and crack front shape upon the resulting K_I values. In his work, he employed singular crack elements with $1/\sqrt{r}$ strain singularity around the crack tip and evaluated the stress intensity factor using the displacement matching method. In order to alleviate the steep stress gradient near the crack tip and due to the limited computational resources at that time, a small radius fillet was introduced at the crack tip. It was found that choosing specimen dimensions such that $a/W > 0.55$ and $(L-a)/W > 0.65$ results in a very close agreement between numerical and analytical K_I predictions (within 5%) in the lower half of the specimen thickness. These results were later confirmed by White [13] using line spring approximate finite element analysis and the same bilinear crack profile to evaluate K_I for the DT specimen. The work of White was further extended to examine the more realistic quarter-ellipse crack profiles and it was found that the analytical estimate in Eq. (1) over estimates K_I values by 10–20%. Tseng and Berry [14] established the following bounds on the validity of the DT test: $L = 2\ W$ and $1/12 \leqslant t/W \leqslant 1/6$. They also

investigated the effect of top and bottom grooves and found the presence of grooves to have marginal effects on the resulting K_I levels.

More recently, Ciccotti and his co-workers [15,16] performed three-dimensional finite element analyses of the DT test using crack advance technique. This technique is particularly accurate and does not impose excessive mesh refinement requirements near the crack tip, yet it is rather demanding in terms of the number of simulations with different crack lengths to evaluate the change in the strain energy release rate (SERR). They studied the influence on the SERR of the specimen width and length, the presence and shape of the bottom groove, the presence of an initial notch, and estimated the curved shape of the fracture front.

The concept of stepped DT specimens aims at deducing the critical stress intensity factor using a single specimen with varying t_c/t ratio, rather than several specimens of different thicknesses. This approach has been implemented experimentally for brittle materials using gray cast iron [17]. The objective of the present study is to investigate the effect of the fracture thickness (t_c) and the number of steps of the stepped DT specimen upon the resulting conditional stress intensity factor using three-dimensional finite element analysis. In the present work, stress intensity factor is evaluated using virtual crack extension approach [18], in which the SERR is evaluated by virtually relocating a set of elements in the immediate vicinity of the crack by a distance of Δa. the main advantage of this technique is that it obviates the need for successive mesh generation to change the crack length to calculate the SERR.

2. Finite element modeling

2.1. Model geometry

The dimensions of both constant-thickness and stepped DT specimens were chosen similar to those in [17,19] to enable comparing the numerical and experimental results. For constant-thickness specimens, the width between the two rollers W_m = 62 mm, length L = 150 mm, and total width W = 75 mm. The specimen is grooved along its longitudinal midplane on both its top and bottom faces. The reduced thickness t_c was varied in order to investigate the effect of the fracture thickness ratio (t_c/t) upon the resulting conditional stress intensity factor K_Q. Table 1 shows the various levels of (t_c/t) under consideration. In total, eight specimens are considered with $0.267 < t_c/t < 0.933$.

Two groups of three- and five-steps DT specimen configurations are considered herein for FEA with their respective geometries and dimensions as depicted in Fig. 2 and Tables 2 and 3. The specimen width between the two rollers is W_m = 100 mm. The minimum thickness t_c in Fig. 2 is varied in intervals along the specimen length such that it is experimentally viable to obtain a series of values of the critical fracture load P_c in Eq. (1) along different length zones in a single specimen, thereby eliminating the need for a multiple of specimens and experiments. The length of each zone L_i was selected to be sufficient to prevent interaction between different zones.

Special attention was devoted to the geometry of the crack front. The actual curved crack front was approximated using a four-segment polyline over the minimum specimen thickness t_c such that the inclination angle increases from 10° to 30° over four equal vertical distances $t_c/4$, as shown in Fig. 3. This approximation has been successfully implemented earlier in [15] and is adopted to overcome three-dimensional mesh generation issues of curved crack fronts.

2.2. Mesh generation

Mesh generation is the most intricate part in the finite element analysis of a crack geometry. The most common technique for crack meshing is to implement a spider-web mesh around the crack front, with quarter-point degenerate quadratic elements on the first row of elements surrounding the crack front. These are modified 20-node three-dimensional solid elements, where the mid-side nodes are shifted towards to the quarter-point near to the crack tip and the element is collapsed into a wedge shape along the crack front. This modification results in a $1/\sqrt{r}$ strain singularity in the element, thereby accurately simulating the physical stress field singularity around the crack tip [12]. Fig. 4 illustrates the mesh design for a five-step DT model with a spider mesh around the crack tip. Away from the crack tip, standard 20-node hexahedral

Table 1
Dimensions of constant-thickness DT cast aluminium specimens.

Specimen	W_m (mm)	t (mm)	t_c/t
ST1-1	62	15	0.27
ST1-2			0.4
ST1-3			0.53
ST1-4			0.67
ST1-5			0.8
ST1-6			0.87
ST1-7			0.9
ST1-8			0.93

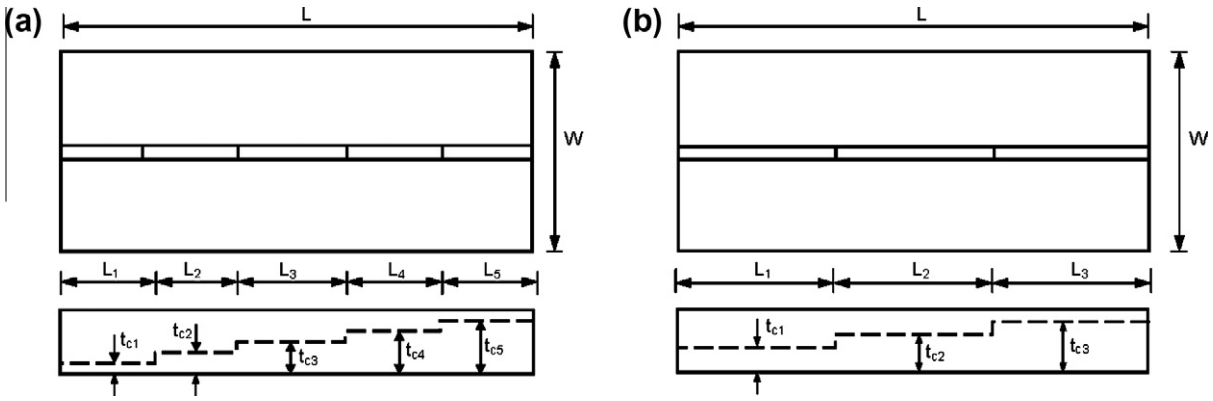

Fig. 2. Schematic of stepped double torsion models: (a) five-step and (b) three-step.

Table 2
Dimensions of three-steps DT grey cast iron specimens.

Specimen	W_m (mm)	t (mm)	t_c/t
ST3-1	100	13	0.35
			0.57
			0.77
ST3-2	100	13	0.69
			0.75
			0.82
ST3-3	100	13	0.85
			0.88
			0.92

Table 3
Dimensions of five-steps DT grey cast iron specimens.

Specimen	W_m (mm)	t (mm)	t_c/t
ST5-1	100	13.5	0.33
			0.47
			0.64
			0.84
			0.96
ST5-2	100	13.6	0.31
			0.56
			0.71
			0.75
			0.91
ST5-3	100	13.6	0.34
			0.59
			0.73
			0.79
			0.92

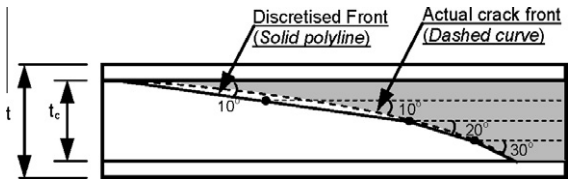

Fig. 3. Polyline discretization of the curved crack front.

elements with three translational degrees of freedom are used. In the present work, mesh generation has been performed using general purpose finite element analysis package [20].

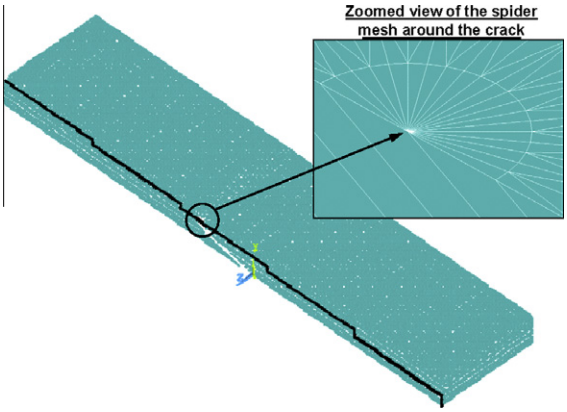

Fig. 4. Mesh generation of ST5-2 five-step DT specimen.

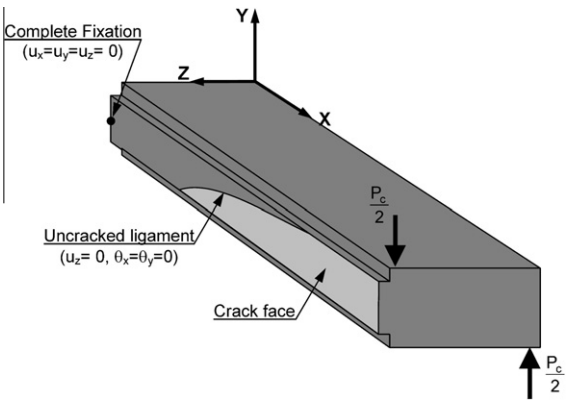

Fig. 5. Schematic drawing of the boundary conditions on half plain DT specimen.

Table 4
Mechanical properties of the specimen materials [17,19].

Material	BHN	UTS (MPa)	Elongation (%)	K_{IC} (MPa $\sqrt{m}$)
Al–Si	45	161.2	2	12.1
Gray CI	190	240	0.45	31.3

2.3. Boundary conditions

The DT specimen geometry and loading conditions depicted in Fig. 1 makes it possible to include only one-half of the specimen in the FE model, as shown in Fig. 5 for the constant-thickness model. Similar conditions can be applied to the stepped model. In this figure, two equal and opposite vertical forces of magnitude $P_c/2$ were applied at the locations of the loading fixture and roller support, respectively, to simulate load control conditions. Symmetry boundary conditions were applied along the uncracked ligament of the specimen such that the nodes on this ligament can only move in the x–y plane. It was sufficient to fully constrain one node on the far end of the model in all directions to prevent rigid body motion; this node was chosen at the midplane of the model as shown in Fig. 5.

2.4. Material properties

The material properties for the finite element simulation were chosen to match those of the experimental work in [17] and [19]. Cast aluminium silicon alloy and gray cast iron were specifically chosen for their low ductility and proximity to brittle fracture behaviour. Table 4 summarizes the mechanical properties of these two alloys. It shows that both alloys exhibit almost negligible ductility and their fracture behaviour is hence expected to be accurately described within the framework of linear elastic fracture mechanics. Furthermore, both materials were assumed to follow a linear elastic isotropic

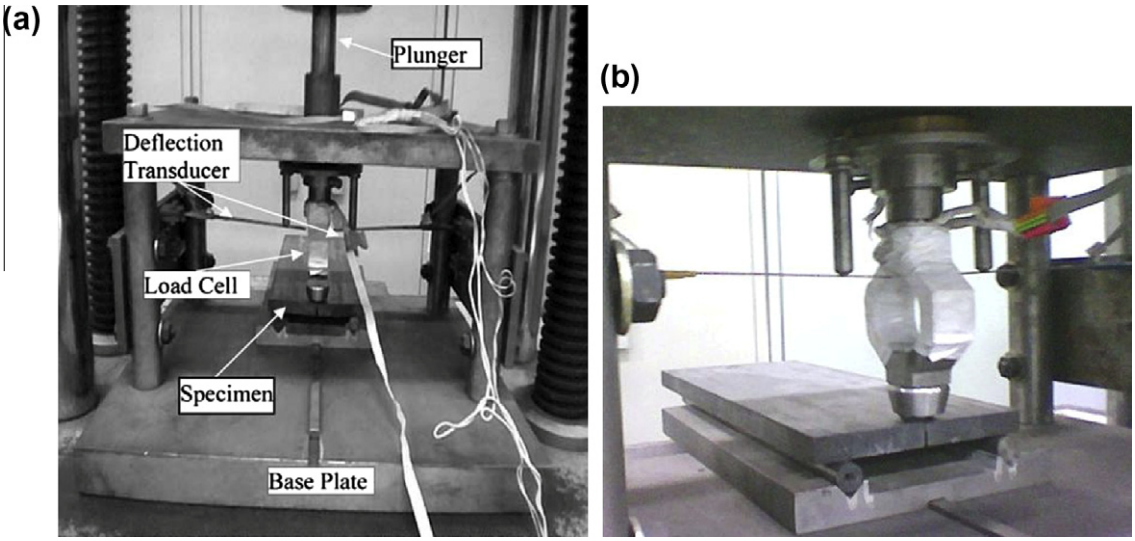

Fig. 6. Double torsion test setup: (a) different setup components and (b) zoomed view of the specimen under load, after [17].

Table 5
Conditional SIF (K_Q) values of uniform-thickness DT model.

Model #	t_c/t	P_c (kN)	K_Q (Exp.) (MPa $\sqrt{m}$)	K_Q (FEA) (MPa $\sqrt{m}$)
ST1-1	0.27	5.2	10.33	8.56
ST1-2	0.4	8.9	14.5	11.01
ST1-3	0.53	11.1	15.63	12.22
ST1-4	0.67	16.1	20.25	16.86
ST1-5	0.8	16.3	18.74	16.27
ST1-6	0.87	12.8	14.08	13.04
ST1-7	0.9	11.5	12.48	11.24
ST1-8	0.93	12	12.73	11.48

behaviour. Experimental evaluation of the plane strain fracture toughness was made using ASTM E399-90 [21] standard three point bend test method. Fig. 6a and b depicts the experimental setup used in [17]. Proprietary load cell and displacement transducer were fabricated and calibrated to ensure high measurement accuracy of the load–displacement pairs. The base plate was mounted on a centering pin on the testing machine to ensure co-axial loading and displacement control test protocol was applied at a constant rate of 1.5×10^{-3} mm. The test specimen was carefully positioned on the supporting rollers to ensure symmetrical loading around the center of the test specimen.

3. Results and discussion

3.1. Uniform-thickness DT model

The conditional stress intensity factor (K_Q) was evaluated analytically and numerically using eight constant-thickness specimens made of cast aluminium. The thickness ratio for these specimens (t_c/t) was gradually increased from 0.27 to 0.93. The analytical plane stress and plane strain estimates are obtained using Eq. (1). The values of K_Q are normalized with respect to standard K_{IC} value obtained using ASTM compact tension specimen (see Table 4). The experimental value of the critical load P_c was used to evaluate K_Q in both the analytical and finite element computations. Table 5 illustrates the variation of P_c with increased t_c/t ratio.

Fig. 7 depicts the variation of normalized K_Q with the fracture thickness ratio (t_c/t) using the calibration equation (plane stress and plane strain) and finite element analysis. In this figure, it is observed that both plane stress and plane strain estimates are very close to each other. In fact, plane strain estimates are higher by a factor of $\sqrt{(1-\nu^2)}$, which amounts to 4.83% in the current problem. It is also observed that all approaches exhibit a similar pattern, in which the values of K_Q gradually increase with (t_c/t) until they reach a peak value at $t_c/t \approx 0.7$. Then, K_Q asymptotically drops to approach the standard K_{IC} value. This pattern can be explained by considering the transition from plane stress to plane strain behaviour. For small t_c/t values, the fracture behaviour is strictly plane stress, and increasing the thickness is associated with a comparable increase in critical load P_c levels. As the specimen critical thickness increases, marked stress triaxiality is observed due to increased constrained material volume, thereby leading to plane strain conditions and associated reduction in K_Q levels.

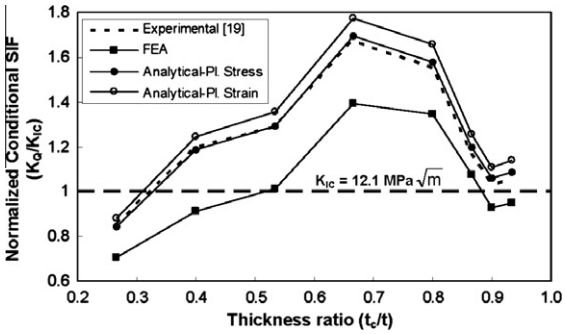

Fig. 7. Normalized conditional SIF (K_Q) predictions using various techniques for uniform-thickness DT specimen.

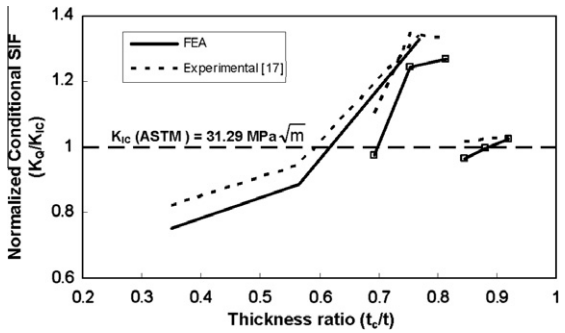

Fig. 8. Normalized conditional SIF (K_Q) predictions using three-step DT specimen.

Table 6
Conditional SIF (K_Q) values of three-step DT model.

Specimen	t_c/t	P_c (kN)	K_Q (Exp.) (MPa $\sqrt{m}$)	K_Q (FEA) (MPa $\sqrt{m}$)
ST3-1	0.35	8.9	25.72	23.55
	0.57	13	29.57	27.78
	0.77	21.5	41.96	41.53
ST3-2	0.69	16	34.46	30.54
	0.75	20.4	42.11	38.94
	0.82	21	41.68	39.67
ST3-3	0.85	16.8	31.88	30.14
	0.88	17.3	32.11	31.22
	0.92	17.8	32.34	32.03

Comparing the plane strain fracture toughness estimates (K_{IC} = 12.1 MPa $\sqrt{m}$) in [19] with K_Q obtained using FEA (11.24 MPa $\sqrt{m}$), a good agreement is observed between both approaches. It is noteworthy to observe that LEFM-based FEA estimates are consistently lower than the experimental values. Aside of common errors in experimental measurements, the most plausible source of discrepancy between these values is the development of a plastic zone around the crack tip, which leads to limited crack blunting. In this case, using *J*-integral, coupled with an elasto-plastic material model, should give a better estimate of the material fracture toughness. Meanwhile, the analytical estimates, both plane stress and plane strain, overestimates K_Q value compared to both experiments results and FE predictions due to the numerous assumptions inherent to this equation. For instance, assuming that the uncracked ligaments of the specimen are rigid artificially stiffens the specimen and yields higher critical fracture load value P_c. This has already been pointed out in an earlier study [15].

3.2. Variable thickness stepped DT model

The conditional stress intensity factor (K_Q) values were evaluated using three- and five-steps DT finite element models having fracture thickness ratios (t_c/t) that range between 0.35 and 0.92. The numerical predictions were compared with the experimental values in [17]. Fig. 8 depicts the variation of K_Q with t_c/t for three-step DT specimens for all ratios considered in Table 2. In this figure, K_Q is normalized with respect to standard K_{IC} value obtained in [17]. Three separate lines indicate three different models, each with a different set of gradually increasing t_c/t. This was necessary to enable comparison of

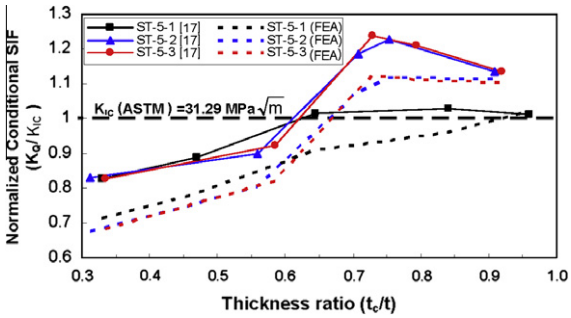

Fig. 9. Normalized conditional SIF (K_Q) predictions using five-step DT specimen.

Table 7
Conditional SIF (K_Q) values of five-step DT model.

Specimen	t_c/t	P_c (kN)	K_Q (Exp.) (MPa $\sqrt{m}$)	K_Q (FEA) (MPa $\sqrt{m}$)
ST5-1	0.33	9.4	25.91	22.27
	0.47	12	27.74	24.52
	0.64	16	31.72	28.44
	0.84	18.5	32.18	30.03
	0.96	19.5	31.63	31.96
ST5-2	0.31	9.2	25.94	21.15
	0.56	13.33	28.09	25.09
	0.71	19.82	37.12	33.64
	0.75	21.19	38.47	35
	0.91	21.5	35.52	34.84
ST5-3	0.34	9.48	25.83	21.35
	0.59	14	28.86	25.66
	0.73	21	38.79	35.18
	0.79	21.44	37.92	34.8
	0.92	21.6	35.51	34.6

experimental and finite element analysis. Similar to the plain double torsion specimens, K_Q value gradually increased with (t_c/t) until it reached its peak value at $t_c/t = 0.769$. Then, K_Q value asymptotically decreased approaching K_{IC} value as $t_c/t \approx 0.846$. Comparing plane strain fracture toughness estimate (31.29 MPa $\sqrt{m}$) obtained [17] with K_Q value using FEA (30.14 MPa $\sqrt{m}$), a good agreement is observed. Furthermore, FEA predictions were in good agreement with the experimental value of the critical stress intensity factor at fracture throughout the thickness range t_c/t under consideration. Table 6 presents a comparison between the K_Q obtained by experimental work in [17] and using FEA.

Fig. 9 depicts the variation of normalized K_Q with t_c/t for five-step DT specimens using both finite element analysis and the experimental values in [17]. The figure presents these results for the three specimens under consideration, shown in Table 3. In contrast to the three-step DT specimens, it was possible here to cover the full range of t_c/t values under investigation (0.33–0.92) using one specimen since the change in t_c/t value over each zone was less abrupt compared to the three-step model. The results show a consistent pattern of K_Q and t_c/t relation, which is similar to that observed in constant-thickness and three-step specimens (see Table 7).

4. Conclusions

In this study, three-dimensional finite element analysis was conducted of constant and variable thickness stepped double torsion specimens. The objective was to obtain the material critical stress intensity factor and to compare it with the plane strain fracture toughness estimates using standard tests. Comparison of numerical and experimental results showed a good agreement between the two approaches for single, three-, and five-steps double torsion specimens. The variation of the conditional stress intensity factor with thickness showed a distinctive pattern of monotonic increase until a thickness ratio of ~0.7 is achieved, after which its value asymptotically approaches the experimental plane strain fracture toughness value. This pattern has been explained in view of mixed plane stress/strain fracture behaviour. Slight deviation existed between numerical and experimental results, which are attributed to the discretised representation of the curved crack front and the development of limited plastic zone ahead of the crack tip, which was not accounted for in the finite element simulations. The results also showed the stepped double torsion test specimen is promising in determining the fracture toughness of the materials, both analytically and experimentally.

References

[1] Outwater JO, Gerry DJ. On the fracture energy of glass. USNL report Contract NONR 3219(01) (X), 1966; AD640848.
[2] Outwater JO, Gerry DJ. On the fracture energy, rehealing velocity and refracture energy of cast epoxy resin. J Adhes 1969;1:290–8.
[3] Kies JA, Clark ABJ. Fracture propagation rates and times to fail following proof stress in bulk glass. In: Pratt PL, editor. Fracture. Proceedings of the 2nd international conference on fracture, London: Chapman and Hall; 1969. p. 483–91.
[4] Tait RB, Fry PR, Garrett GG. Review and evaluation of the double-torsion technique for fracture toughness and fatigue testing of brittle materials. Exp Mech 1987;27:14–22.
[5] Shyam A, Lara-Curzio E. The double-torsion testing technique for determination of fracture toughness and slow crack growth behavior of materials: a review. J Mater Sci 2006;41:4093–104.
[6] Murphy MC, Kumble RG, Berry JT, Outwater JO. Fracture toughness in cast metals. Am Foundry Soc Trans 1973;81:158–62.
[7] Williams DP, Evans AG. A simple method for studying slow crack growth. J Test Eval 1973;1(4):264–70.
[8] Evans AG. A method for evaluating the time-dependent failure characteristics of brittle materials and its application to polycrystalline alumina. J Mater Sci 1972;7:1137–46.
[9] Timoshenko SP. Theory of elasticity. 3rd ed. McGraw Hill Publishers; 1970.
[10] Fuller Jr ER. An evaluation of double torsion testing: analysis. In: Freiman SW, editor. Fracture mechanics applied to brittle materials – ASTM STP 678.
[11] Radovic E, Lara-Curzio E. Mechanical properties of tape cast nickel-based anode materials for solid oxide fuel cells before and after reduction in hydrogen. Acta Mater 2004;52:5747–56.
[12] Trantina CG. Stress analysis of the double torsion specimen. J Am Ceram Soc 1977;60(7–8):338–41.
[13] White CS. Line-spring analysis of the double-torsion specimen. Engng Fract Mech 1984;19(4):751–3.
[14] Tseng AA, Berry JT. A three-dimensional finite element analysis of the double torsion test. J Press Vess Technol Trans ASME 1979;101:328–35.
[15] Ciccotti M. Realistic finite-element model for the double-torsion loading configuration. J Am Ceram Soc 2000;83(11):2737–44.
[16] Ciccotti M, Negri N, Gonzato G, Mulargia F. Practical application of an improved methodology for the double torsion load relaxation method. Int J Rock Mech Mining Sci 2001;38:569–76.
[17] Essa GMF, Radwan AA, Adly MA. Validation of double torsion test with a single stepped-thickness specimen in determination of fracture toughness. In: Abdel-Mageed T, Megahed SM, editors. Proceedings of the 9th Cairo University international conference on mechanical design and production (MDP-9), Egypt: Cairo University Press; 2008. pp. 483–92.
[18] Delorenzi HG. On the energy release rate and the J-Integral of 3-D crack configurations. Int J Fract 1982;19:183–93.
[19] Adly MA. Factors affecting fracture toughness using double torsion test. M.Sc. Thesis, Cairo University; 1984.
[20] ANSYS release 10 theory manual; 2005.
[21] ASTM E399-90. Standard test method for plane-strain fracture toughness of metallic materials. American society for testing of materials; 1990.